Breakdown of Dirac dynamics in honeycomb lattices due to nonlinear interactions

Omri Bahat-Treidel, Or Peleg, and Mordechai Segev
Department of Physics, Technion-Israel Institute of Technology, Technion City, Haifa IL-32000, Israel

Hrvoje Buljan
Department of Physics, University of Zagreb, PP 332, HR-10000 Zagreb, Croatia
(Received 26 April 2010; published 26 July 2010)

We study the dynamics of coherent waves in nonlinear honeycomb lattices and show that nonlinearity breaks down the Dirac dynamics. As an example, we demonstrate that even a weak nonlinearity has major qualitative effects on one of the hallmarks of honeycomb lattices: conical diffraction. Under linear conditions, a circular input wave packet associated with the Dirac point evolves into a ring, but even a weak nonlinearity alters the evolution such that the emerging beam possesses triangular symmetry, and populates Bloch modes outside of the Dirac cone. Our results are presented in the context of optics, but we propose a scheme to observe equivalent phenomena in Bose-Einstein condensates.

DOI: 10.1103/PhysRevA.82.013830 PACS number(s): 42.65.−k

The past decade has witnessed considerable interest in honeycomb lattices in many fields, ranging from carbon nanotubes [1] and graphene [2–4] in condensed matter, cold atoms in honeycomb optical lattices [5–8], and electromagnetic waves in honeycomb photonic crystals [9–12] and photonic lattices (waveguide arrays) [13–15]. The unique features of the honeycomb lattice result from its unusual band structure, displaying two intersecting bands. The vicinity of the intersection points is conical, and excitations residing at the close vicinity of the intersection points obey the massless Dirac equation: a relativistic wave equation for massless spin-half particles. As a consequence of this unusual linear dispersion and the additional degrees of freedom (two sites in each unit cell, referred as pseudospin), a variety of exciting phenomena have been obtained: room-temperature quantum Hall effect in graphene [16], conical diffraction in honeycomb photonic lattices [13], negative magnetoresistance implying antilocalization [17–19], and Klein tunneling [15,20–22], to name a few. The dynamics of Dirac-like excitations in honeycomb lattices has been well studied when the propagation equation is linear (interaction-free). However, the dynamics can also be nonlinear, as happens in the optical domain due to light-matter interactions and for atomic Bose-Einstein condensates (BECs) due to pairwise scattering. In either of these, the nonlinear dynamics has received little attention in the context of honeycomb lattices. The first study of nonlinear dynamics in honeycomb lattices was conducted in [13], demonstrating gap solitons, which had no overlap with Bloch modes residing in the vicinity of the Dirac points. Later studies of nonlinear dynamics in honeycomb lattices were a generalization of the Dirac approximation [23–25], where a nonlinear version of the massless Dirac equation was studied.

Here we study the nonlinear dynamics of waves in honeycomb lattices, where initial wave packets are composed of Bloch waves from the vicinity of the Dirac points. Such wave packets are very well described by the massless Dirac equation. However, even the presence of a fairly weak nonlinearity drives the waves away from the vicinity of the Dirac points; hence the nonlinearity breaks the Dirac dynamics associated with honeycomb lattices. We demonstrate this dramatic change in the dynamics by investigating conical diffraction: an initial wave packet with circular symmetry that evolves into two concentric rings (separated by a dark ring). Surprisingly, under slightly nonlinear conditions, the same (circular) input beam evolves into a triangular-ring beam. Interestingly, we find that the resulting triangle is rotated by π when the nonlinearity changes sign; that is, a given input beam subjected to a focusing nonlinearity (attractive interactions for BECs) evolves into a triangle that is rotated by π with respect to the triangle obtained when the same input beam is subjected to a defocusing nonlinearity (repulsive interactions for BECs). Hence, the presence of nonlinearity (interactions) changes the wave dynamics in honeycomb lattices dramatically, introducing important changes to the unique phenomena associated with the effective Dirac equation, such as conical diffraction and Klein tunneling. Moreover, the nonlinear breakdown the Dirac dynamics, in itself, gives rise to interesting new effects. Our results are presented in the context of optics; however, we propose a scheme to observe equivalent phenomena in BECs.

The paraxial propagation of a monochromatic field envelope ψ inside a photonic lattice with Kerr nonlinearity is described by

$$i\frac{\partial\psi}{\partial z} = -\frac{1}{2k}\nabla_\perp^2\psi - \frac{k\delta n(x,y)}{n_0}\psi - \frac{k}{n_0}n_2|\psi|^2\psi, \qquad (1)$$

where $\delta n(x,y)$ is the modulation in the refractive index defining the lattice as shown in Fig. 1(a), k is the wave number in the medium, n_0 is the background refractive index, and n_2 is the Kerr coefficient. The sign of n_2 determines the type of nonlinearity, where $n_2 > 0$ corresponds to a focusing nonlinearity (attractive interactions in the context of BECs). The term $k\delta n/n0$ is referred to as the optical potential.

At low intensities ($n_2|\psi|^2 \ll \max\{\delta n(x,y)\}$), the nonlinear term is negligible and the propagation can be described by linear methods. In the absence of the nonlinear term, Eq. (1) has solutions of the form $\psi(x,y,z) = U(x,y)\exp(i\beta z)$, where $U(x,y)$ is a solution of the eigenvalue equation

$$\hat{H}_0 U(x,y) = \beta U(x,y), \quad \text{where} \quad \hat{H}_0 \equiv -\frac{1}{2k}\nabla_\perp^2 - \frac{k}{n_0}\delta n(x,y), \qquad (2)$$

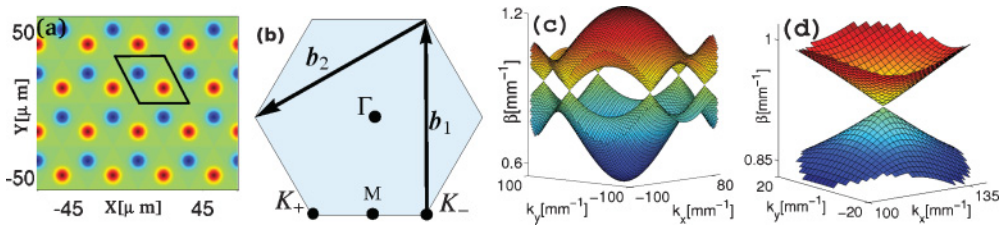

FIG. 1. (Color online) (a) Perfect honeycomb lattice that has two sites in a unit cell. (b) The first Brillouin zone with the high symmetry points. (c) The first two bands. (d) The vicinity of the intersection (Dirac) point.

and the eigenvalue, β, is the propagation constant (analogous to the energy in quantum mechanics with opposite sign, that is, $\beta \leftrightarrow -E$). Since $\delta n(x,y)$ is a periodic function in x and y, the eigenfunctions of $\hat{H}_0$ can be chosen to be Bloch waves

$$B_{\boldsymbol{q},m}(\boldsymbol{r}) = u_{\boldsymbol{q},m}(\boldsymbol{r}) \exp(i\boldsymbol{q}\cdot\boldsymbol{r}), \tag{3}$$

where $u_{\boldsymbol{q},n}(x,y)$ has the same periodicity as the potential, $\boldsymbol{q} = (q_x,q_y)$ is the lattice momentum, $\boldsymbol{r} = (x,y)$ is the transverse coordinate, and m is the band index. We solve numerically Eq. (2) in the first Brillion zone (BZ) [Fig. 1(b)] and obtain the band structure $\beta(\boldsymbol{q})$ [Fig. 1(c)]. Note the intersection of the bands at the corners of the first BZ. According to Fig. 1(a), it appears as if there are six intersection points; however, these six points are in fact two triplets of two nonequivalent points denoted by $K_\pm$ [Fig. 1(b)]. That is, there are only two nonequivalent intersection points, since the corners are connected by reciprocal lattice vectors [Fig. 1(b)]. The close vicinity of the intersection points is conical [Fig. 1(d)]. In the tight binding approximation, the effective Hamiltonian describing the Bloch modes from the vicinity of these points is the Dirac Hamiltonian for massless particles [26]. Hence, these points are often referred to as *Dirac points*, and the band structure in the vicinity of these points forms *Dirac cones*. We emphasize that Bloch modes that reside outside the Dirac cone cannot be described by the Dirac equation, since the propagation constant $\beta(\boldsymbol{q})$ is no longer linear in $\boldsymbol{q}$, and moreover it does not possess circular symmetry but rather a threefold symmetry (as will be discussed later).

Our main interest in the article is the effect of nonlinearity on the extremely unique diffraction pattern, named *conical diffraction,* obtained for an input beam composed of Bloch modes residing in the Dirac cone. Conical diffraction refers to the fact that at a large enough propagation distance, the circular (envelope) input beam evolves into two bright rings of constant width separated by a dark ring and a vanishing intensity at the origin [13,14]. A characteristic conical diffraction pattern is shown in Fig. 2(b), where the first ring is separated from the second ring that is just starting to form (for two distinct rings see [14]). Experimentally, the input beam can be constructed by means of a spatial light modulator (SLM) or by three plane waves with wave vectors corresponding to the three equivalent corners (say K_+) of the BZ [14].

At high intensities, the nonlinear term comes into play. The input wave packet has an envelope that possesses circular symmetry. Hence, the optical potential induced through the nonlinear term has circular symmetry as well. The initial excitation is around the Dirac points, where the Dirac cone approximation is excellent. Thus, one could expect that, even though some qualitative differences would emerge, the resulting diffraction pattern would still have circular symmetry. This educated guess is supported by analysis of the "nonlinear Dirac equation" (Dirac equation with a nonlinear term) [23]. We test this idea by solving Eq. (1) numerically using the split-step Fourier algorithm in the presence of a focusing nonlinearity, where the input beam is composed of Bloch modes from the vicinity of the point K_+. We construct the input beam using $\boldsymbol{k}\cdot\boldsymbol{p}$ approximation

$$\psi(\boldsymbol{r},0) = \sqrt{\mathcal{N}}[B_{K_+,1}(\boldsymbol{r}) + iB_{K_+,2}(\boldsymbol{r})]\exp(-\boldsymbol{r}^2/\sigma^2), \tag{4}$$

where $B_{K_+,1}(\boldsymbol{r})$ and $B_{K_+,2}(\boldsymbol{r})$ are the two degenerate Bloch modes corresponding to the K_+ point, σ is the width of the envelope, and $\mathcal{N}$ determines the beam's power. Surprisingly, we find that the diffraction pattern contradicts these expectations by having a threefold symmetry [Fig. 2(c)]: instead of the circular rings we obtain a triangle pointing to the right. Even more surprising is the diffraction pattern

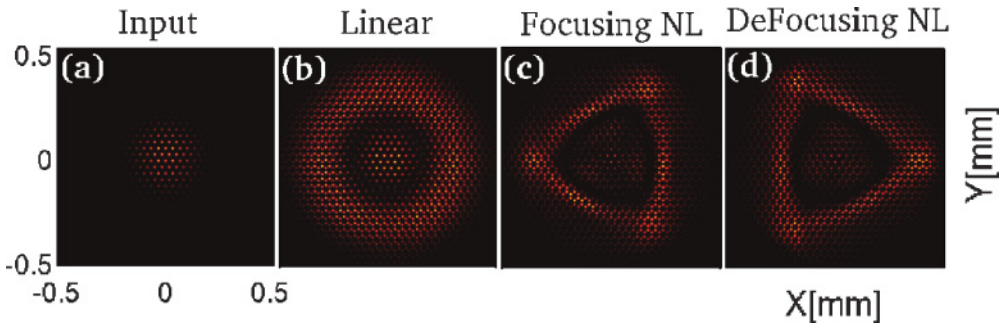

FIG. 2. (Color online) (a) Input beam from the vicinity of K_+. (b) The output of the linear propagation. (c) The output of the nonlinear propagation with focusing nonlinearity. (d) The output of the nonlinear propagation with defocusing nonlinearity.

obtained when the sign of the nonlinearity is reversed: defocusing instead of focusing [Fig. 2(d)]. In the defocusing case, the emerging triangular diffraction pattern is almost identical to the focusing case, but is rotated by π. The values of the parameters used in the simulation are $D = 35$ (μm), where D is the lattice constant, $\max\{\delta n\} = 7 \times 10^{-4}$, $\max\{n_2|\psi|^2\} = 5 \times 10^{-5}$, $n_0 = 1.5$, $k = 7.85 \times 10^6$ (m^{-1}), and the propagation distance $Z = 8$ (cm).

We find another interesting phenomenon by repeating the numerical experiment with a similar input beam that is centered around the other nonequivalent Dirac point K_-: the orientation of the triangle is reversed again. In other words, for a focusing nonlinearity, similar input beams centered around the different Dirac points evolve into triangles that are mirror images of each other. We emphasize that the π rotation of the intensity pattern that results from the different Dirac points is *exact*, as opposed to the π rotation resulting from reversing the sign of the nonlinearity. In the latter case, the orientations of the triangles are indeed rotated, but the intensities are not identical, as can be seen from Figs. 2(c) and 2(d). Therefore, even though similar physical effects are obtained, their physical origin is different.

In all these simulations, we find that the width of the "triangular ring" is *smaller* than the width of the circular ring (arising in the linear case), for both types (signs) of nonlinearity. This result is surprising since generally the focusing and the defocusing nonlinearities have opposite effects on the width of the propagating wave packet. Namely, in a homogeneous medium, the former will always decrease the width of a finite beam, whereas the latter will increase it. These opposite tendencies occur also in periodic structures, where the action on the beam width is determined by the sign of the nonlinearity with respect to the sign of the effective mass; for example, in regions of anomalous diffraction (negative effective mass) a focusing nonlinearity always broadens the beam, whereas defocusing narrows it, etc. As stated previously, the honeycomb lattice is also unique in the sense that the expansion of the evolving triangular ring beam is not affected by the sign of nonlinearity; the width of the ring decreases for both cases [Figs. 2(c) and 2(d)]. Moreover, the mean radius of the triangular ring beam, defined as

$$R \equiv \sqrt{\langle\psi(z)|(x^2+y^2)|\psi(z)\rangle}, \tag{5}$$

is the same for the linear and nonlinear diffraction patterns; that is, the mean radius of the evolving beam is not affected by the weak nonlinearity at all. The results of the numerical experiment can be summarized as follows.

(1) The nonlinearity transforms conical diffraction into triangular diffraction.

(2) The wave packet evolves into a triangular ring for both focusing and defocusing nonlinearity, and nonlinearities of opposite signs result in similar triangles pointing to opposite directions.

(3) Two identical wave packets centered around different Dirac points yet subject to the same nonlinearity evolve to identical triangular rings pointing in opposite directions.

The rest of the article presents our explanation of these unexpected observations that cannot be explained simply by adding a nonlinear term to the Dirac equation.

In order to analyze the dynamics, we write the wave function as a linear combination of Bloch modes (Bloch decomposition):

$$\psi(\boldsymbol{r},z) = \sum_m \int_{\mathrm{BZ}} d^2q\, B_{\boldsymbol{q},m}(\boldsymbol{r}) g_m(\boldsymbol{q},z), \tag{6}$$

where $g_m(\boldsymbol{q},z)$ is the amplitude of each Bloch mode and $B_{\boldsymbol{q},m}(\boldsymbol{r})$ is a Bloch wave defined in Eq. (3). Substituting the expansion of ψ into Eq. (1) it is clear that the nonlinear term mixes four Bloch waves with different lattice momenta, $\boldsymbol{q}$; that is, the nonlinear term generates spatial four-wave-mixing and therefore the output beam may include Bloch modes that were not initially populated. Hence, even though the input beam is very localized in k space around the Dirac point, it does not necessarily remain localized during the propagation. In fact, in previous theoretical and experimental work in nonlinear photonic lattices it was clearly shown that the Bloch population grows by virtue of four-wave-mixing [27], and in some cases it even leads to spatial supercontinuum [28].

More quantitative analysis of the nonlinear evolution of the distribution of Bloch modes reveals the underlying physics of the triangular diffraction pattern. The population of the m^{th} band is defined as

$$P_m \equiv \int_{\mathrm{BZ}} d^2q\, |\langle\psi(z)|B_{\boldsymbol{q},m}\rangle|^2 = \int_{\mathrm{BZ}} d^2q\, |g_m(\boldsymbol{q},z)|^2, \tag{7}$$

and the population imbalance between the first two bands is given by

$$\Delta(z) = P_1 - P_2 = \int_{\mathrm{BZ}} d^2q\, [|g_1(\boldsymbol{q},z)|^2 - |g_2(\boldsymbol{q},z)|^2]. \tag{8}$$

We calculate the projections of the input and output beams on the Bloch waves of the first two bands and find very interesting results: the Bloch distribution $|g_m(\boldsymbol{q},0)|^2$ of the initial beam has circular symmetry (as expected), with no population imbalance, whereas the Bloch distribution of the output beam $|g_m(\boldsymbol{q},Z)|^2$ has **threefold symmetry** with a significant population imbalance. Figure 3 presents the evolution of the Bloch distribution for the beam of Fig. 2 and the population in each band, for both types of nonlinearity. Clearly, focusing nonlinearity increases the population in the first band at the expense of the second band, thereby generating a positive imbalance, whereas defocusing nonlinearity generates a negative imbalance. While calculating the imbalance, $\Delta(z)$, during the propagation we find that it is generated only in the early stages of the propagation [Fig. 4(a)]. Moreover, the final imbalance increases with the power of the beam [Fig. 4(b)].

This analysis leads to three main conclusions:

(1) The nonlinearity gives rise to population transfer to Bloch modes that reside outside the Dirac cone; hence, *nonlinearity breaks the Dirac dynamics.*

(2) The sign of nonlinearity determines the direction of population transfer.

(3) The Bloch distribution of the output beam always has threefold symmetry in k-space; hence, it is clear that the intensity in real space has threefold symmetry as well.

These conclusions can be explained by more fundamental arguments, where the most crucial step is to understand why

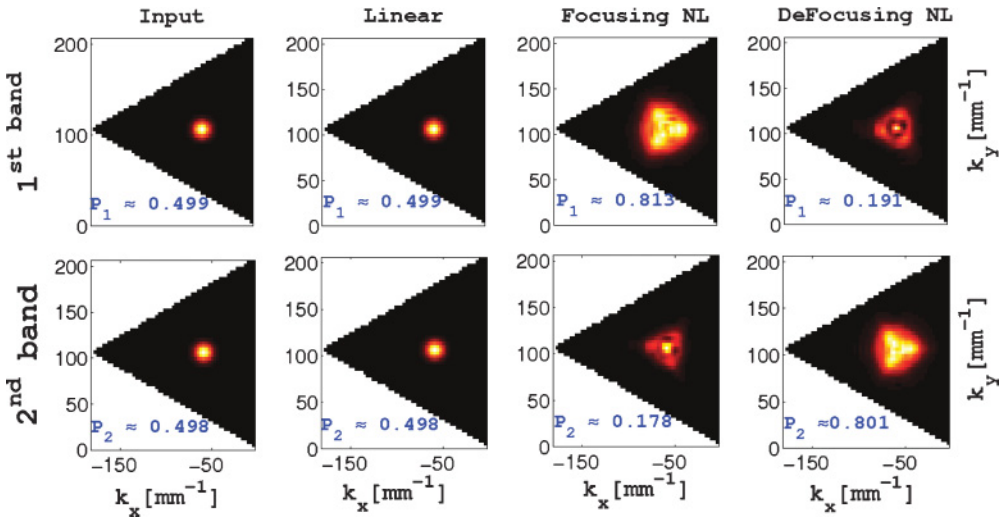

FIG. 3. (Color online) The Bloch mode decomposition of the input wave packet from the vicinity of the Dirac point. (a)–(d) The Bloch distribution of the first band $|g_1(\boldsymbol{q})|^2$. (e)–(h) The Bloch distribution of the second band $|g_2(\boldsymbol{q})|^2$. In each figure we write the corresponding population. Clearly, focusing nonlinearity transfers the energy to the first band, and defocusing nonlinearity transfers the population to the second band.

the nonlinearity generates a population imbalance between the bands. In order to do so, consider the functional

$$\mathcal{H}_{cl}(z) = \mathcal{H}_L + \mathcal{H}_{NL}, \tag{9}$$

where

$$\mathcal{H}_L \equiv -\int \left(\frac{1}{2k} |\nabla_\perp \psi|^2 - \frac{k}{n_0} \delta n(x,y) |\psi|^2 \right) d^2x, \tag{10}$$

$$\mathcal{H}_{NL} \equiv \int \frac{k}{2n_0} n_2 (|\psi|^2)^2 d^2x. \tag{11}$$

Note that $\mathcal{H}_{cl}$ is a constant of motion; that is, $\partial_z \mathcal{H}_{cl} = 0$. The evolution equation, Eq. (1), is derived from $\mathcal{H}_{cl}$ via the variational principle:

$$i\frac{\partial \psi}{\partial z} = -\frac{\delta \mathcal{H}_{cl}}{\delta \psi^*}. \tag{12}$$

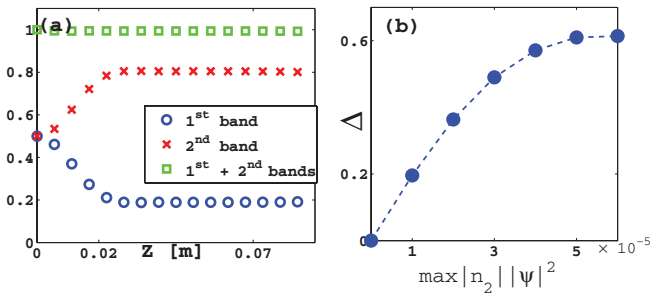

FIG. 4. (Color online) (a) The population in the first two bands during the propagation in the presence of defocusing nonlinearity, where $\max\{|n_2||\psi|^2\} = 4 \times 10^{-5}$. (b) The final population imbalance as a function of the strength of the nonlinear refractive index.

It is instructive to note that $\mathcal{H}_L$ can be interpreted as the mean propagation constant of the wave packet in the absence of nonlinearity:

$$\mathcal{H}_L(z) = \langle \psi(z) | \hat{H}_0 | \psi(z) \rangle = \sum_{m=1,2} \int_{\mathrm{BZ}} d^2q \beta_m(\boldsymbol{q}) |g_m(\boldsymbol{q},z)|^2. \tag{13}$$

Since $\mathcal{H}_{cl}$ is a constant of motion, we can write

$$\mathcal{H}_L(0) + \mathcal{H}_{NL}(0) = \mathcal{H}_L(z) + \mathcal{H}_{NL}(z). \tag{14}$$

The initial beam is constructed around the Dirac point with equal population of both bands. Since the bands are almost symmetric, from Eq. (13) we find that $\mathcal{H}_L(0)$ equals the propagation constant at the Dirac point, β_D. Since the spectrum can be shifted by a constant without affecting the dynamics, we can set $\mathcal{H}_L(0) = \beta_D = 0$. During the propagation the beam experiences significant broadening, and since the total power is conserved, the amplitude of the wave packet decreases with z. Hence, the nonlinear contribution to $\mathcal{H}_{cl}$ becomes negligible compared to the linear contribution at large z; that is, $\mathcal{H}_{NL}(z) \ll \mathcal{H}_L(z)$. Therefore Eq. (14) simplifies to

$$\mathcal{H}_L(z) \simeq \mathcal{H}_{NL}(0) = \int \frac{k}{2n_0} n_2 (|\psi|^2)^2 d^2x, \tag{15}$$

thus the sign of $\mathcal{H}_L(z)$ is identical to the sign of n_2. By substituting Eq. (13) and using the symmetry of the bands, $\beta_2(\boldsymbol{q}) \approx -\beta_1(\boldsymbol{q})$, we obtain

$$\mathcal{H}_{NL}(0) \simeq \int_{BZ} d^2q \beta_1(\boldsymbol{q}) [|g_1(\boldsymbol{q},z)|^2 - |g_2(\boldsymbol{q},z)|^2]. \tag{16}$$

Since $\beta_1(\boldsymbol{q})$ is positive (first band), the sign of $\mathcal{H}_{NL}(0)$ is the same as the final population imbalance; hence the nonlinearity determines the direction of population transfer between the bands. From Eqs. (15) and (16) it is clear that positive n_2 (focusing nonlinearity) yields a positive population imbalance; that is, after a fairly large propagation distance, the first

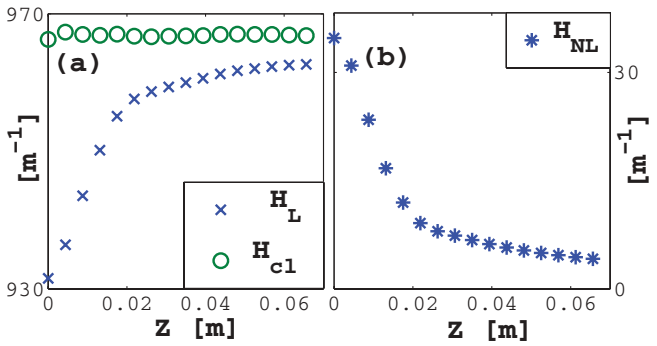

FIG. 5. (Color online) (a) Calculation of $\mathcal{H}_{cl}(z)$ and $\mathcal{H}_L(z)$ in the presence focusing nonlinearity. (b) The nonlinear contribution to $\mathcal{H}_{cl}(z)$, which decreases rapidly during the propagation.

band has a greater population. For both signs of nonlinearity the resulting Bloch distributions are very similar. However, since the group velocity of the bands differs in sign, the orientations of the resulting triangles are rotated by π with respect to each other. We emphasize that, other than creating a population imbalance and broadening the Bloch distribution, the different signs of nonlinearity have the same physical effect, as opposed to other systems. The arguments given previously are supported by numerical calculation of $\mathcal{H}_L$ and $\mathcal{H}_{NL}$ during the propagation, as presented in Fig. 5. Notice that most of the population transfer occurs during the early stages of propagation—just like the population imbalance shown in Fig. 4(a), and with the same characteristic length.

Now that we understand that the distribution of Bloch modes varies during propagation, we turn to understanding the resulting threefold symmetry. We reexamine the bands around the Dirac point by plotting a contour of $\beta(\boldsymbol{q})$ as shown in Fig. 6 and find that, very close to the Dirac point, $\beta(\boldsymbol{q})$ has circular symmetry, but further away it has threefold symmetry. Since the new distribution of the Bloch modes follows $\beta(\boldsymbol{q})$, the resulting distribution also has threefold symmetry. This argument explains the Bloch distribution of the output beam, implying that the intensity in real space also has a threefold symmetry. Due to z-reversal symmetry, $\beta(\boldsymbol{q}) = \beta(-\boldsymbol{q})$, implying that the contours of equal $\beta(\boldsymbol{q})$ around the point K_+ are mirror images of the contour lines around the point K_-. Therefore, the Bloch distribution and hence the real-space intensity resulting from the different Dirac cones are exact mirror images of each other.

Next, we try to give a more intuitive explanation for the spatial intensity pattern, based on the transverse group

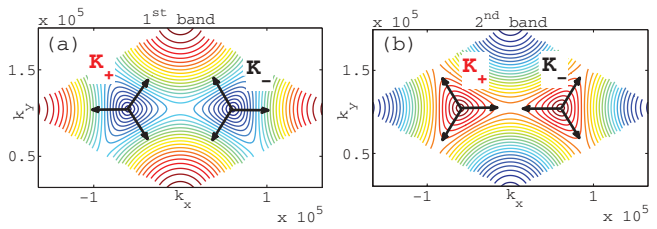

FIG. 6. (Color online) Contour plot of the first two bands. The Dirac points are denoted by $K_\pm$. The black arrows point in the directions where the group velocity is maximal.

velocity defined as $\boldsymbol{v}_g \equiv \nabla_{\boldsymbol{q}}\beta(\boldsymbol{q})$, which is in fact the angle of propagation. The input beam populates a region in k space in which $\beta(\boldsymbol{q})$ has circular symmetry, and all waves propagate with a transverse group velocity of the same magnitude in the radial direction. Since the nonlinearity (say, focusing, where we have shown that the nonlinear dynamics is determined by the structure of the first band) causes the Bloch distribution to expand in k space and leave the Dirac cone, some of the modes propagate with a greater group velocity than others. After some propagation distance, these modes are mapped in real space to the most distant points which are the vertices of the triangle in real space. From Fig. 6 it is clear that around the different Dirac points the directions of maximal group velocity are opposite. Therefore, a beam centered around K_+ with focusing nonlinearity evolves into a triangle pointing to the right, whereas the similar input beam centered around K_- with focusing nonlinearity evolves into a triangle pointing to the left [Fig. 6(a)]. This explains why similar input beams around the different Dirac points subjected to the same nonlinearity evolve into triangles pointing in opposite directions.

When the same input beam is subjected to nonlinearity of the opposite sign, the wave packet expands in k space as well. However, for the opposite sign of nonlinearity, the energy is transferred to the opposite band (as explained earlier). The contour lines of both bands are almost identical, but the group velocity has an opposite sign (Fig. 6), and therefore the corners of the intensity triangle (in real space) are again opposite to each other. Therefore, an input beam centered around K_+ (K_-) with *focusing* nonlinearity evolves into a triangular ring beam pointing to the left (right), whereas when the same input beam is subjected to a *defocusing* nonlinearity it evolves into a triangle pointing to the right (left).

Up to this point the breakdown of Dirac dynamics was considered in the context of optics. However, we predict the existence of identical phenomena in the context of ultracold atomic BECs, based on the fact that Eq. (1) describes dynamics of an interacting BEC in a honeycomb potential. Such potentials can be constructed optically; however, they were considered mainly in the context of fermionic gases (e.g., see Refs. [5–8]), probably because electrons in real graphene are fermions, for which the ground state is a filled Fermi sea up to the Fermi level (which can be shifted from the Dirac point depending on doping), and because the ground state of a Bose gas in a potential with graphene band structure is not a condensate occupying Bloch modes in the vicinity of the Dirac point. Thus, in order to obtain such a state one should do it dynamically. Here we propose a scheme which is not trivial, but still realistic experimentally: Suppose that one prepares a finite-size condensate in a harmonic, pancake-shaped, effectively two-dimensional trap [29]. At some point in time, the in-plane confinement is turned off (the confinement keeping the 2D structure is still present), the pancake BEC is subsequently given a momentum kick with three plane waves with angles $2\pi/3$ with respect to each other, which are directed into the three equivalent corners of the BZ (say K_+), and then the honeycomb potential is ramped up (the lattice spacing of the honeycomb potential should be much smaller than the size of the cloud). The initial BEC can be noninteracting, and the nonlinearity can be turned on via the

Feshbach mechanism (say when the honeycomb potential is ramped up). Such an experimental sequence of events is not an easy task but it is within today's experimental capabilities. The sign of the nonlinearity and the strength of the interactions can be tuned for some BECs by a Feshbach resonance mechanism.

In conclusion, honeycomb lattices possess intersection points between the first two bands, and Bloch modes that reside close to these points give rise to extremely unique dynamics: dynamics of massless spin-half particles described by the Dirac equation. We have shown that, in the presence of nonlinearity, this unique dynamics is significantly altered and the Dirac equation is no longer suitable for describing the (propagation) evolution. In addition, we have studied the nonlinear evolution of wave packets composed of such Bloch modes, which under linear conditions yield conical diffraction. We have found that both signs of nonlinearity transform the circular rings into triangular rings, resulting in a triangular diffraction pattern. This new type of diffraction cannot be obtained simply by adding the nonlinear term into the effective Dirac equation, since the Bloch modes' distribution quickly expands beyond the range of the Dirac cone, where the effective evolution equation governing the dynamics cannot be approximated by the Dirac equation nor by its nonlinear extension. Hence we expect that the intriguing phenomena obtained in honeycomb lattices, such as Klein tunneling, *Zitterbewegung* [30,31], antilocalization, zero mode edge-states [32,33], and more, would be significantly altered by the presence of nonlinearity. Likewise, the intriguing features related to Dirac points in photonic crystals [9–12] would be affected by nonlinearities of the same type studied here.

ACKNOWLEDGMENTS

This work is supported in part by the Croatian-Israeli scientific collaboration funded by the Ministries of Science in both countries and by an advanced grant from the ERC. H.B. acknowledges support from the Croatian Ministry of Science (Grant No. 119-0000000-1015).

[1] S. Iijima, Nature (London) **354** 56 (1991).
[2] Y. Zheng and T. Ando, Phys. Rev. B **65**, 245420 (2002).
[3] K. S. Novoselov *et al.*, Nature (London) **438**, 197 (2005).
[4] V. P. Gusynin and S. G. Sharapov, Phys. Rev. Lett. **95**, 146801 (2005).
[5] C. Wu, D. Bergman, L. Balents, and S. Das Sarma, Phys. Rev. Lett. **99**, 070401 (2007).
[6] S.-L. Zhu, B. Wang, and L. M. Duan, Phys. Rev. Lett. **98**, 260402 (2007).
[7] C. Wu and S. Das Sarma, Phys. Rev. B **77**, 235107 (2008).
[8] K. L. Lee, B. Gremaud, R. Han, B. G. Englert, and C. Miniatura, Phys. Rev. A **80**, 043411 (2009).
[9] F. D. M. Haldane and S. Raghu, Phys. Rev. Lett. **100**, 013904 (2008).
[10] R. A. Sepkhanov, Y. B. Bazaliy, and C. W. J. Beenakker, Phys. Rev. A **75**, 063813 (2007).
[11] R. A. Sepkhanov, J. Nilsson, and C. W. J. Beenakker, Phys. Rev. B **78**, 045122 (2008).
[12] T. Ochiai and M. Onoda, Phys. Rev. B **80**, 155103 (2009).
[13] O. Peleg, G. Bartal, B. Freedman, O. Manela, M. Segev, and D. N. Christodoulides, Phys. Rev. Lett. **98**, 103901 (2007).
[14] O. Bahat-Treidel, O. Peleg, and M. Segev, Opt. Lett. **33**, 2251 (2008).
[15] O. Bahat-Treidel, O. Peleg, M. Grobman, N. Shapira, M. Segev, and T. Pereg-Barnea, Phys. Rev. Lett. **104**, 063901 (2010).
[16] K. S. Novoselov *et al.*, Science **315**, 1379 (2007).
[17] S. V. Morozov, K. S. Novoselov, M. I. Katsnelson, F. Schedin, L. A. Ponomarenko, D. Jiang, and A. K. Geim, Phys. Rev. Lett. **97**, 016801 (2006).
[18] E. McCann, K. Kechedzhi, V. I. Falko, H. Suzuura, T. Ando, and B. L. Altshuler, Phys. Rev. Lett. **97**, 146805 (2006).
[19] F. V. Tikhonenko, A. A. Kozikov, A. K. Savchenko, and R. V. Gorbachev, Phys. Rev. Lett. **103**, 226801 (2009).
[20] T. Ando, T. Nakanishi, and R. Saito, J. Phys. Soc. Jpn. **67**, 2857 (1998).
[21] A. K. G. M. I. Katsnelson and K. S. Novoselov, Nature Phys. **2**, 620 (2006).
[22] A. F. Young and P. Kim, Nature Phys. **5**, 222 (2009).
[23] M. J. Ablowitz, S. D. Nixon, and Y. Zhu, Phys. Rev. A **79**, 053830 (2009).
[24] L. H. Haddad and L. D. Carr, Phys. D **238**, 1413 (2009).
[25] L. H. Haddad and L. D. Carr, e-print arXiv:1006.3893v2 [cond-mat.quant-gas] (2010).
[26] G. W. Semenoff, Phys. Rev. Lett. **53**, 2449 (1984).
[27] O. Manela, G. Bartal, M. Segev, and H. Buljan, Opt. Lett. **31**, 2320 (2006).
[28] R. Dong, C. E. Ruter, D. Kip, O. Manela, M. Segev, C. Yang, and J. Xu, Phys. Rev. Lett. **101**, 183903 (2008).
[29] Z. Hadzibabic and J. Dalibard, e-print arXiv:0912.1490v2 [cond-mat.quant-gas] (2009).
[30] M. Katsnelson, Eur. Phys. J. B **51**, 157 (2006).
[31] T. M. Rusin and W. Zawadzki, Phys. Rev. B **80**, 045416 (2009).
[32] K. Nakada, M. Fujita, G. Dresselhaus, and M. S. Dresselhaus, Phys. Rev. B **54**, 17954 (1996).
[33] M. Kohmoto and Y. Hasegawa, Phys. Rev. B **76**, 205402 (2007).